Numerical Investigation of Cavity Geometry and Tilt Angle Effects on Cooling and Electrical Efficiency of PV-PCM Systems

Youness Bannour[1], *Yassine* El Alami[2], *Hanane* Chetnouf[2], *Anas* Hassari[3], *Kamal* Hirech[3], *Ahmed* Faize[1], *Bachir* Benhala[4] and *Elhadi* Baghaz[2]

[1]Mathematics and Information Systems Laboratory, Department of Physics, Polydisciplinary Faculty of Nador, Selouane, Morocco.
[2]Laboratory of Electronics, Instrumentation and Energetic, Faculty of Sciences, Chouaib Doukkali University, El Jadida, Morocco.
[3]Higher School of Technology - LGEM Laboratory, Mohammed First Univesity, Oujda, Morocco.
[4]Faculty of Sciences Dhar El Mahraz Fez, Sidi Mohamed Ben Abdellah University, Fez, Morocco.

Abstract. This research investigates numerically the impact of cavity geometry and tilt angle on the thermal and electrical performances of PV-PCM systems. Two configurations of semi-elliptical cavities, elongated and wide, are studied at two tilt angles of 10° and 30° using the enthalpy-porosity approach in the ANSYS Fluent code. The results show that increasing the tilt angle leads to significant improvements in natural convection within the PCM, leading to improved melting time, temperature uniformity and cooling efficiency. Of the four cases examined, the elongated cavity at 30° induced tilt (case 2) had the best thermal performance, with an average temperature reduction of approximately 8.6 K, compared to the least effective configuration. The melting ratio improved by almost 21%, showing a marked improvement in the heat transfer and phase change characteristics. The electrical efficiency improved from 10.38 to 10.95%, which is a relative improvement of 5.5%. The above results indicate the strong coupling between cavity geometry and inclination angle and PV solar energy temperature control and higher efficiency potential of optimized PV-PCM configurations greater photovoltaic efficiency. Future work will include verification through experimentation of this study and consider the investigation of other cavity configurations and PCM materials which can improve system performance.

1 Introduction

The rapid increase of photovoltaic (PV) technology has increased interest worldwide in the improved efficiency and durability of solar energy systems. However, the efficiency of the conversion of PV modules is greatly influenced by the temperature at which they operate [1], as excess heat buildup reduces their electrical performance and accelerates the deterioration of material properties [2]. In order to resolve this difficulty, a number of passive and active cooling systems have been studied, of which the incorporation of PCMs has shown great promise. PCMs can absorb and store excess thermal energy during the melting process, thereby stabilizing the temperature of the PV cells and increasing their electrical efficiency. Increased heat transfer and melting behaviour of PCM have been the focus of much research. Bria et al. [3] demonstrated that changing the PCM thickness significantly affects the cooling efficiency of PV modules, with a cooling potential of over 32 °C being achieved. Abdelmoneim et al. [4] and Maghrabi et al. [5] experimentally illustrated that enlarging the tilt angle and optimising the thickness of the PCM would improve the melting rate and electrical efficiency by about 14%. Similarly, in the work by Amalu et al. [6] voltage improvements of 10.8% in electrical efficiency were gained from the pairing of PCM coolers and silicon PV cells. Further developments here have included geometric and structural changes with finned and porous PCM arrangements aiming to improve heat transfer. Nižetić et al. [7] and Akshayveer et al. [8] have confirmed that multi-container and fin-assisted PCM systems obtained power output increases of over 10%. The introduction of metals, foams or nanoparticles in the PCM, as examined by Klemm et al. [9] and Stalin et al. [10], was responsible for uniform melting and improved thermal response, emphasising the importance of internal geometry on PCM efficiency. More recently, Bannour et al. [11] have managed to optimise numerically the fin arrays used in PV-PCM systems through a detailed analysis of fin number and length using the enthalpy–porosity method, enabling analysis within ANSYS Fluent. Their findings indicate that increasing fin density produces much improved melting rate and electrical output with values of efficiency improvement of about 5.8% being achieved, compared with the least optimised design. This was an important step towards identifying the major geometric parameters that dominate heat transfer and energy conversion in PV-PCM systems. Although a number of studies have been conducted into PV-PCM systems, little research is available evaluating the influence of the cavity geometry and tilt angle of the PV panel on melting of the PCM, and thermal performance. The geometry of the cavity and the angle of inclination of the panel will influence the natural convection and heat distribution and thus affect the efficiency of the system. In this study, the effects of two semi-elliptical cavity geometries (elongated and wide) and two angle of inclination of the panel (10° and 30°) upon the thermal and electrical performance of PV-PCM systems is investigated numerically using the enthalpy–porosity method in ANSYS Fluent, with the aim of finding the optimum design parameters for improved heat transfer and power output.

2 Physical arrangement

2.1 Specification Overview

The system under investigation consists of a module PV and a layer of PCM placed below it, acting as a thermal regulator to lower the temperature of the PV cells, leading to improved electrical values. Two geometric configurations of the PCM layer were designed in order to study the effect of the shape of the cavity on the heat transfer and the melting processes. The first configuration consists of elongated semi-elliptical cavities, located below the absorber, while the second configuration consists of cavities of larger semi-elliptical shape. These cavities will act as adiabatic or nearly adiabatic regions that were intended to direct the heat flow path and modify natural convection patterns of the PCM during the melting process, having a direct impact on the temperature distribution of the PV panel and hence its electrical efficiency. Both configurations were tested under two inclination angles of (10° and 30°) to see the effect of inclination on the thermal and electrical performance of the system and the melting fraction of the PCM. The selected geometric configurations and inclination angles provide a reasonable compromise between simplicity of design and thermal-electrical performance efficiency, which can give a better insight into the joint effect of cavity geometry and inclination angle on the cooling characteristics, melting process, and efficiency of the system PV-PCM. Table 1 presents layers properties and thermophysical properties of the system, while Table 2 outlines the PCM properties. The schematic description of the system configured according to the two configurations adopted is shown in Figure 1.

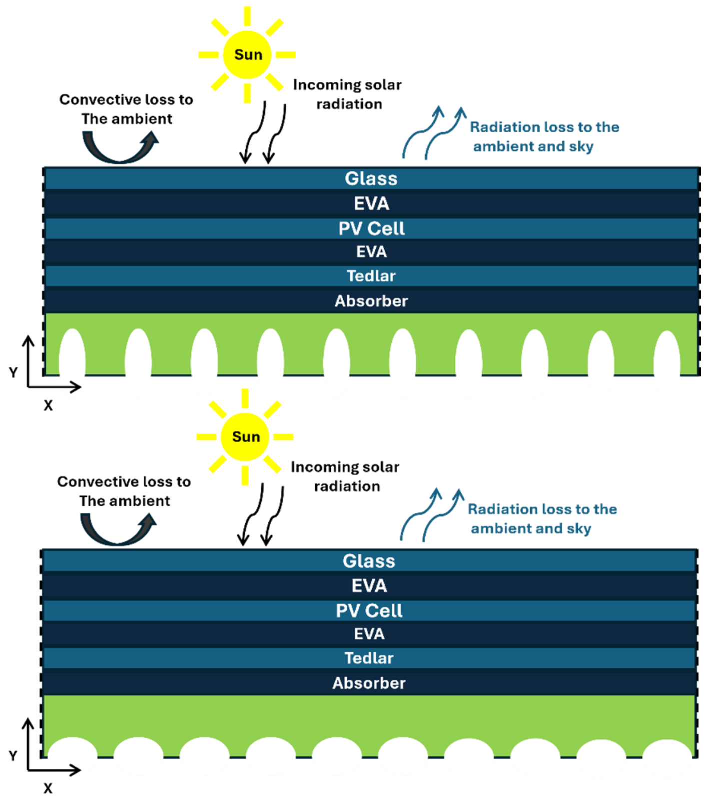

Fig. 1. Schematic representation of two PV-PCM systems with different semi-elliptical cavity shapes (elongated and wide).

Table 1. PV-PCM layers properties, used as input data in the numerical model *[12]*.

Material	Thickness (mm)	C (J/kg.K)	K (W/m.K)	ρ (kg/m³)
Absorber	2	817	202.4	2719
Tedlar	0.1	1250	0.2	1200
EVA	0.5	2090	0.35	960
Solar cell	0.3	700	100	2330
Glass	4	786	1.5	2650
PCM	30	2000	0.2	820

Table 2. Paraffin RT42 PCM's properties.

Property	Paraffin RT42
Fusion enthalpy (J/kg)	174000
Dynamic viscosity (kg/m.s)	0.02351
Melting Temperature (K)	313.15
Thermal expansion coefficient (1/K)	0.0005

2.2 Hypotheses and Governing Equations

Optimization techniques are based on assumptions that are intended to decrease the computational cost while minimizing errors. The following assumptions were taken to simplify the numerical model:

- The physical properties of the solid components (the PV layers and the absorber within the PCM) do not depend on temperature [13].
- The Boussinesq approximation is implemented [14].
- Gravity acts along the negative Y-axis direction.
- The lateral and bottom boundaries of the unit are considered adiabatic sides [15].
- The sky temperature (T_{sky}) is the temperature of a blackbody [16].
- Each transient simulation is run for a duration of 2 hours, and the mean electrical output is computed over that duration.
- The solar radiation is assumed uniform and absorbed within the glass layer of the PV module [17].
- The EVA layer is treated as perfectly transparent (100% transmissivity) [18].
- The thermal contact resistance between the PV and PCM solid interfaces is considered negligible [19].

The PV-PCM unit's governing equations are formulated as follows:

2.2.1 Solid Components

The transfer of heat in the solid parts of the system, which includes glass, EVA, solar cell, Tedlar, and heat sink, is primarily through thermal conduction. The governing energy equation for each of these layers can be written as follows:

$$\rho C_{p,s} \frac{\partial T_s}{\partial t} = \nabla . (k_s \nabla T_s) \tag{1}$$

2.2.2 PCM

The enthalpy-porosity method was utilized to model the melting of PCM capturing phase change effects in the energy equation by an apparent enthalpy and porosity factor, simplifying computations while maintaining accuracy [20]:

- Formula for mass conservation:

$$\frac{\partial \rho}{\partial t} + \nabla.(\rho.V) = 0 \tag{2}$$

- Momentum equation:

$$\rho\left[\frac{\partial \vec{V}}{\partial t} + (\vec{V}.\nabla)\vec{V}\right] = -\nabla \mathrm{P} + \nabla.(\mu\nabla\vec{V}) + S \tag{3}$$

$$S = \frac{(1-\beta)^2}{(\beta^3 + \emptyset)} A_{mush}(\vec{V} - \vec{V_p}) \tag{4}$$

A parameter β (0 for solid, 1 for liquid) governs the PCM phase, and the mushy zone ($A_{mush} = 10^5$) is the intermediate state. Solid velocity ($\vec{V_p}$) is material movement in the material frame, and a small constant φ = 0.001 ensures a stable numerical performance.

- Equation of Energy:

$$\frac{\partial(\rho H)}{\partial t} + \nabla.(\rho\vec{V}H) = \nabla.(k\nabla T) + S \tag{5}$$

The symbols H, S, ρ, and $\vec{V}$ denote total enthalpy, source term, density, and velocity, and are used to characterize energy and momentum transfer in the PCM. Total enthalpy (H) serves to represent both sensible and latent heat when a phase change occurs, and is modeled as follows:

$$H = h + \Delta H \tag{6}$$

In this equation, ΔH and h refer to, respectively, the latent and sensible enthalpy, where the latter is given by:

$$h = h_{ref} + \int_{Tref}^{T} C_p dT \tag{7}$$

In this case, h_{ref} is the reference enthalpy calculated at a reference temperature ($Tref$), for the latent enthalpy is presented like so:

$$\Delta H = \beta L \tag{8}$$

The PCM's latent heat (L) varies between 0 and L. The molten fraction (β) is expressed according to the following relation:

$$\beta = \begin{cases} 0 & if\ T \leq\ T_{solidus} \\ \dfrac{T - T_{solidus}}{T_{liquidus} - T_s} & if\ \ T_{solidus} \leq T \leq T_{liquidus} \\ 1 & else\ \ T \geq T_{liquidus} \end{cases} \tag{9}$$

2.3 Initial and boundary conditions

The operating conditions were established at 300 K with a constant heat flux of (1000 W/m^2) imposed on the upper surface of the PV panel [21]. The side and lower walls are considered to be perfectly insulated. Heat losses to the ambient occur via natural convection and radiation and the heat dissipating from the glazed surface is calculated as:

$$\dot{q}_{loss} = h_w^*(T_w - T_s) + \sigma\varepsilon\left(T_{sky}^4 - T_s^4\right) \tag{10}$$

In this relation, h_w^* , σ , and ε denote the wind convective coefficient, the Stefan–Boltzmann constant, and the surface emissivity respectively, which are needed to evaluate heat exchange between the PV module and the environment by wind, surface, and sky (denoted by ' w ', 's', and ' sky ' respectively). The heat transfer coefficient associated with wind, as referenced in Eq. (10), is evaluated as follows [22]:

$$\begin{aligned} h_w^* &= 5.70 + 3.8\,V_w \quad if\ V_w < 5\ \frac{m}{s} \\ h_w^* &= 6.47 + (V_w)^{0.78} \quad if\ V_w > 5\ \frac{m}{s} \end{aligned} \tag{11}$$

Here, V_w denotes the wind velocity. Moreover, the sky temperature treated as a black body in Eq. (10) is calculated using the expression given in [8]:

$$T_{sky} = 0.0522.\,T_{amb}^{1.5} \tag{12}$$

where T_{amb} is the ambient temperature.

The other model components' surfaces are similarly defined with interface boundary conditions.

2.4 Numerical Method and Grid Selection

The simulation was conducted on a computer equipped with a quad-core processor and 16 GB of RAM, consuming about five hours in terms of computational time for a physical simulation of tree hours and 52 minutes. The simulation was executed at 50 iterations per time step to warrant stable solutions. A quadrilateral-dominant mesh was used, comprising 10,662 elements, with a relatively high element quality of 0.885 and an aspect ratio of 1.82, providing sufficient spatial resolution (Figure 2). The numerical simulation was conducted using ANSYS Fluent 19.2, whereby the melting of the PCM was modeled with the enthalpy method and the porosity model to fine-tune the phase change behavior. The energy and momentum equations were solved with the Second-Order Upwind scheme; for the pressure velocity coupling, the PISO algorithm was used with the PRESTO pressure scheme for added accuracy. The use of sub-relaxation factors and enforcing strict convergence criteria-maintained stability throughout the simulations, which, in this study, assessed the PCM effect on the thermal dynamics of the PV panel.

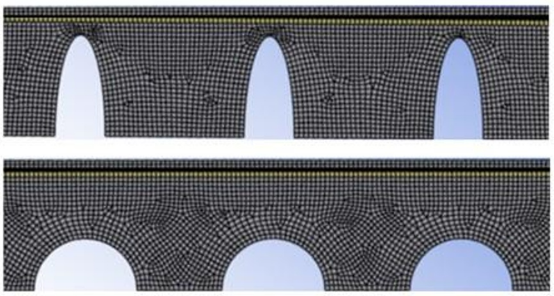

Fig. 2. Mesh configuration of the two PV-PCM system geometries used in the thermal analysis.

2.5 Thermodynamic analysis

This study assesses the PV-PCM system performance via energy analysis based on the first law of thermodynamics. The effective absorbed solar radiation $\dot{E}_{eff,sun}$, is calculated as follows [23]:

$$\dot{E}_{eff,sun} = \tau_g \alpha_{sc} p_{sc} \dot{E}_{sun} A_{PV} \quad (13)$$

where τ_g is the glass transmissivity, p_{sc} the solar cell packing factor, α_{sc} the cell absorptivity, A_{PV} the PV area, and $\dot{E}_{\text{sun}}$ the total incident solar radiation rate.

The following formula is used to calculate the electrical efficiency of the PV-PCM system:

$$\eta_{el} = \frac{\dot{E}_{el}}{\dot{E}_{eff,sun}} = \eta_r . [1 - 0.0045. (T_{cell} - 298.15)] \quad (14)$$

where, η_r stands for the performance of the PV module under standard test conditions (STC) temperature of the PV cells, which can affect the performance and overall energy conversion efficiency.

3 Results and discussion

The temperature contours shown in Figure 3 indicate how cavity geometry and orientation of panels affect heat transfer in PCM. In all cases, the maximum temperature occurs directly under the PV layer and above the upper surface of the PCM where solar heat is received. With a 10° angle of tilt (Cases 1 and 3), heat transfer is predominately by conduction and there is little circulation, leading to local hot spots. Case 1 (long cavity) has a temperature of 344.32 K whilst Case 3 (wide cavity) has a maximum temperature of 344.62 K indicating that there is little natural convection at small angles of tilt. As the angle of tilt is increased to 30° (Cases 2 and 4) then the flow produced by the buoyancy is increased. In Case 2 it is seen that there is a well defined plume inclined in the direction of the flow and the lowest temperature (339.75 K) occurs, whilst in the case of Case 4 the uniformity is seen to be increased with a moderate temperature of 341.63 K at the maximum. In all cases, increasing the angle of tilt is seen to lead to better convection, a reduction in the temperature gradient, and a reduction in the temperature of the PV surface. The long cavity with an angle of tilt of 30° gives rse to the best uniformity in the cooling.

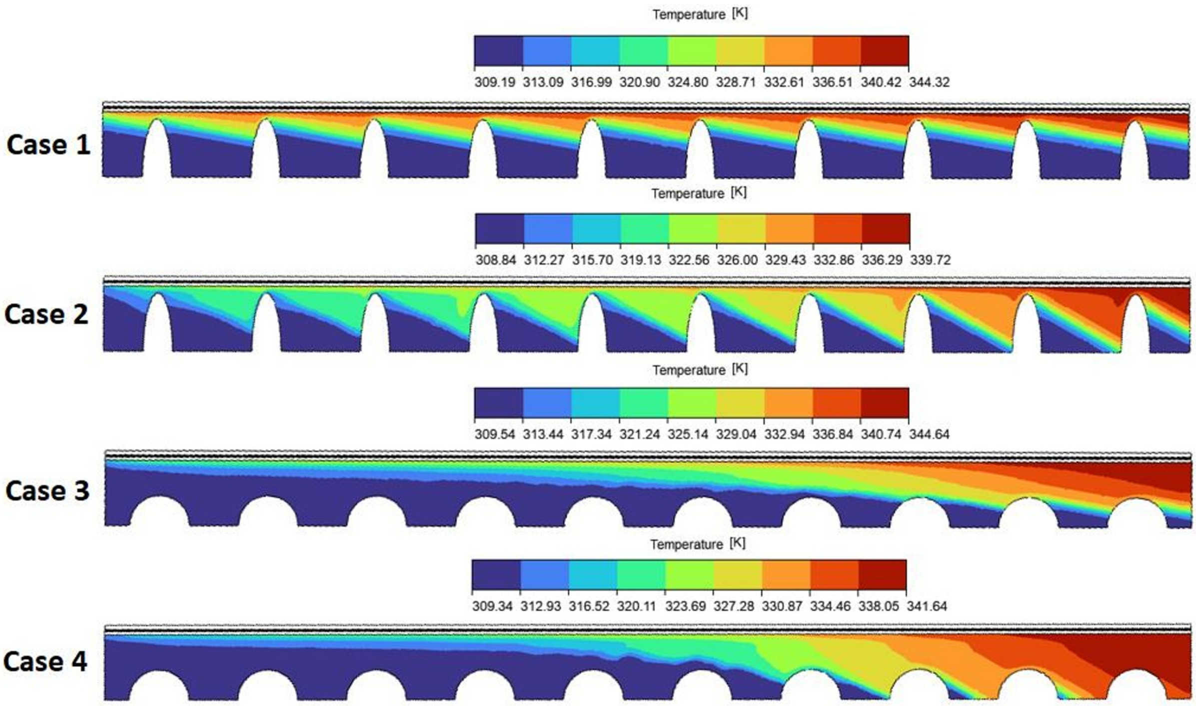

Fig. 3. Temperature contours within the PCM layer for four different semi-elliptical cavity configurations (Case 1–Case 4) in the inclined PV-PCM system.

Figure 4 shows the melt fraction of the PCM through the four configurations. Melting occurs near the top interface below the PV layer and proceeds downwards through conduction and natural convection. At an inclination of 10° (Cases 1 and 3) the process is primarily conduction dominated, leading to a slow melting of the PCM and small areas of liquid. The long cavity (Case 1) shows a reduced melted area, whilst the wide cavity (Case

3) has less vertical heat transfer due to stagnant areas. When the inclination is increased to 30° (Cases 2 and 4) convection due to buoyancy becomes stronger in its action producing inclined melting fronts and hastening the phase change. The best melt fraction (Case 2) occurs at a 30° inclination of the long cavity (≈0.63). The second best melt fraction is for case 4, the wide cavity (≈0.60), cases 1 and 3 (10° inclinations) remaining below a melt fraction of 0.55. Overall a higher inclination improves convection effects and melting uniformity, Case 2 (long cavity 30°) proving to be the best performer thermally in the PV-PCM system.

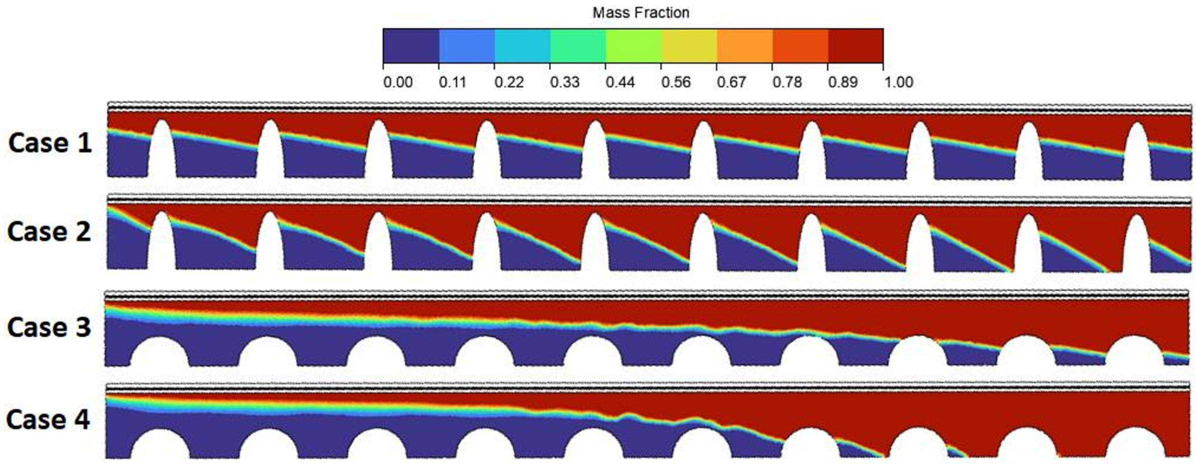

Fig. 4. Mass fraction contours within the PCM layer for four different semi-elliptical cavity configurations (Case 1–Case 4) in the inclined PV-PCM system.

The transient evolution of the temperature of the PV module is represented in Figure 5 for the four analyzed cases. All configurations show a typical two-stage thermal response, characterized in the initial heating period (0 - 2000 s) by a rapid rise of temperature, followed by a slow stabilization when the PCM starts to melt and absorb latent heat. For the angles of 10° (Cases 1 and 3), the PV module reaches a higher steady-state temperature of approximately342.9 K and 336.9 K, respectively, which shows that conduction is the predominant heat transport mode, with a limited convective effect. Conversely, for 30° tilt (Cases 2 and 4), the heat transfer by buoyancy-driven convection will improve and the temperature realized will be lower and equal to 334.3 K and 333.2 K, respectively. Conclusively, it can be stated that the increase of the inclination guarantees a more efficient convective circulation of the heat carrier (PCM), allows therefore a better heat removal from the PV module, consequently lower temperature and greater thermal stability of the module. The best performance with regard to cooling is provided by the long cavity with 30° inclination (Case 2), which results in an average temperature reduction of almost 8.6 K with respect to the baseline configuration (Case 1).

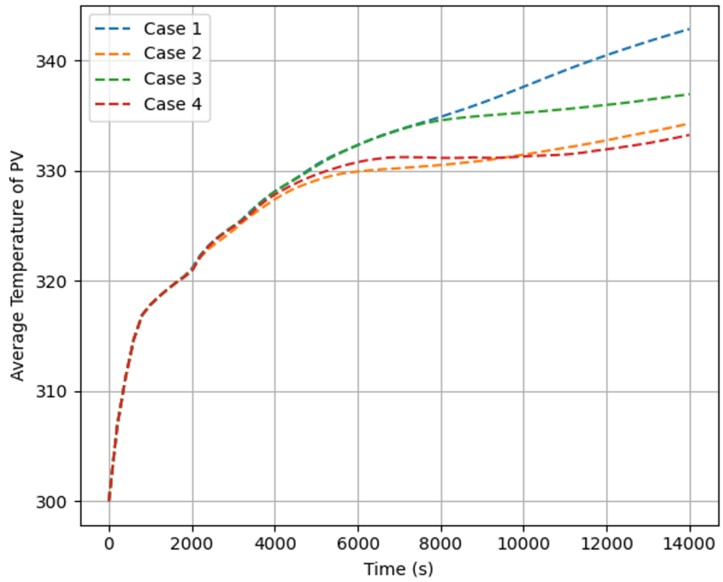

Fig. 5. Average PV temperature over time for four cavity configurations (Cases 1–4).

Figure 6 presents the time evolution of the melted PCM fraction, for the four configurations analyzed. All cases show a 3-phase melting process, dominated at initial stages by conduction (0 - 2000 s), followed by a quasi-linear increase, dominated by natural convection (2000 - 10,000 s) and finished with a gradual stabilization corresponding to the thermal equilibrium of the system. For the inclination of 10° (Cases 1 and 3) the melting process occurs more slowly, due to the weak buoyancy forces, obtaining final melted fractions of 0.52 and 0.56 respectively. The increase of the inclination to 30° (Cases 2 and 4) stimulates the natural convection motion and augmented the heat transfer within the PCM, obtaining final fractions of 0.63 and 0.59 respectively. This behavior shows how the inclination and the geometry of the cavity can determine the phase change phenomena. A higher inclination improves the natural convection stimulating the melting process and improving the temperature uniformity. The long cavity at 30° (Case 2) presents the most efficient melting process, since it absorbs the heat more in a faster way, promoting the better use of latent heat and a better final cooling efficiency of the PV-PCM system.

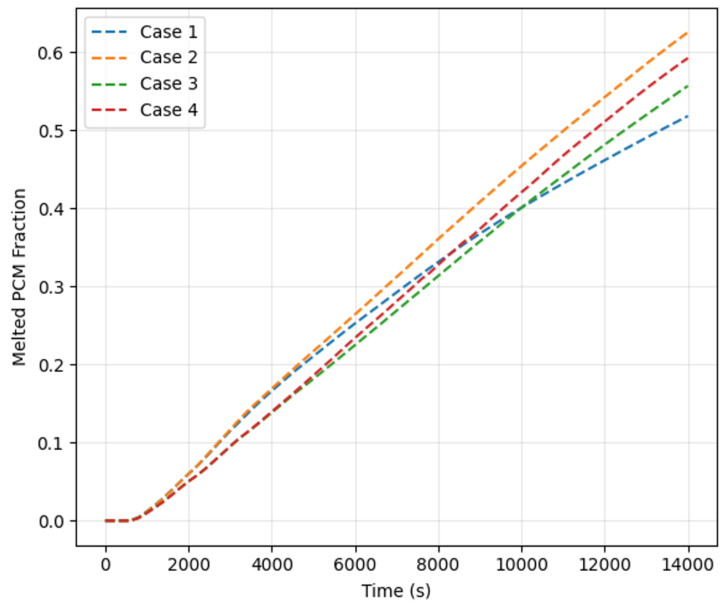

Fig. 6. Average PV temperature over time for four cavity configurations (Cases 1–4).

Figure 7 depicts the variation of the electrical performance as a function of time: for all four configurations considered, an initial rapid decrease in efficiency occurs during the early heating phase due to the fast rise in PV temperature; this is followed by a slower reduction in efficiency after melting of the PCM commences, since then the absorption of the heat supplied to the PCM takes place by latent heat of melting. For the elongated cavity cases (Cases 1, 2) with tilt angles of 10° and 30°, respectively, the greater the angle of inclination, the more vigorous the natural convection effects are manifested in the PCM mass, thus resulting in a decrease in the temperature of the PV receiver and a small improvement in electrical performance. For the wide cavity cases (Cases 3, 4) the thermal performance is made more stable and a slower decrease in efficiency again results. At the end of the run of the simulation the performances are found to attain efficiency values in the vicinity of 10.38%, 10.89%, 10.73%, and 10.95% for Cases 1 to 4, respectively. These performances show that by far the best cooling and electrical result is obtained with the wide cavity and maximum tilt angle employed (30°), and that the elongation of cavity at 10° (Case 1) suffers the maximum temperature disadvantage owing to its high thermal stresses and attendant low efficiency.

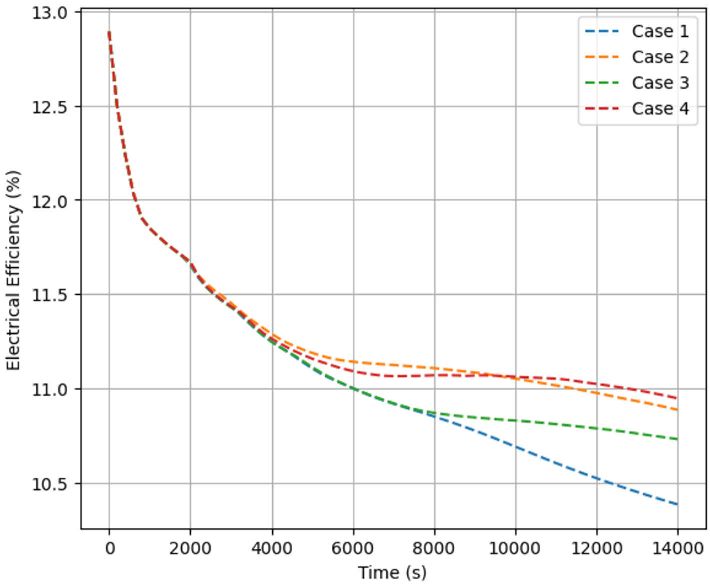

Fig. 7. Electrical efficiency over time for different tilt angles (Cases 1–4).

4 Conclusion

The numerical investigation carried out in this study clearly showed that the geometry of the cavity and the inclination angle are important factors in the thermal and electrical performance of the PV-PCM systems. Natural convection in the PCM was improved by increasing the inclination angle leading to a more uniform temperature distribution and faster melting results. Of all the configurations considered the elongate cavity and the inclination angle 30º (Case 2) gave the higher thermal performance reducing the average temperature of the PV by some 8.6 K from the value of the temperate case. In respect of melting of the PCM the increase in performance from the least efficient configuration Case 1 to the most efficient Case 2 was approximately 21.2 %, which reflected increased convection heat transfer and speed of phase change. With respect to electrical performance the efficiency increased from 10.38 % to 10.95 % corresponding to the electrical output increase of about 5.5 %, which is a measure of the relative performance from the lowest to the highest performing cases. It is clear from these results that there is a close coupling between the geometry and the position of these systems in the efforts to optimise both heat transfer and conversion of energy in PV-PCM systems. Future studies will encompass this work so that validation of the totals by experimental methods may be achieved by evaluation of other types of cavity structure and PCM materials so as to improve further the total performance of the system.

5 References

[1] Y. El Alami, E. Baghaz, R. Nasrin, M. Al-Damook, R. Bendaoud, T. Bouragba, M. Melhaoui, M. Benhmida, Up-to-Date Review on Flat-Plate Solar Hybrid Photovoltaic Thermal Systems: Absorber Designs and Fabrication Materials, Int. J. Energy Res. 2025 (2025) 5547555. https://doi.org/10.1155/er/5547555.
[2] Y. El Alami, Y. Bannour, F. Ouerradi, H. Chetnouf, A. Ghennioui, B. Benhala, E. Baghaz, C. Hajjaj, Experimental and numerical evaluation of the performance of a photovoltaic panel in a semi-arid climate,

in: 2025 5th Int. Conf. Innov. Res. Appl. Sci. Eng. Technol. IRASET, IEEE, Fez, Morocco, 2025: pp. 1–6. https://doi.org/10.1109/IRASET64571.2025.11008049.

[3] A. Bria, B. Raillani, D. Chaatouf, M. Salhi, S. Amraqui, A. Mezrhab, Effect of PCM thickness on the performance of the finned PV/PCM system, Mater. Today Proc. 72 (2023) 3617–3625. https://doi.org/10.1016/j.matpr.2022.08.409.

[4] A.R. Abdulmunem, P. Mohd Samin, H. Abdul Rahman, H.A. Hussien, I. Izmi Mazali, H. Ghazali, Numerical and experimental analysis of the tilt angle's effects on the characteristics of the melting process of PCM-based as PV cell's backside heat sink, Renew. Energy 173 (2021) 520–530. https://doi.org/10.1016/j.renene.2021.04.014.

[5] H.M. Maghrabie, A.S.A. Mohamed, A.M. Fahmy, A.A. Abdel Samee, Performance enhancement of PV panels using phase change material (PCM): An experimental implementation, Case Stud. Therm. Eng. 42 (2023) 102741. https://doi.org/10.1016/j.csite.2023.102741.

[6] E.H. Amalu, O.A. Fabunmi, Thermal control of crystalline silicon photovoltaic (c-Si PV) module using Docosane phase change material (PCM) for improved performance, Sol. Energy 234 (2022) 203–221. https://doi.org/10.1016/j.solener.2022.02.001.

[7] S. Nižetić, M. Jurčević, D. Čoko, M. Arıcı, A novel and effective passive cooling strategy for photovoltaic panel, Renew. Sustain. Energy Rev. 145 (2021) 111164. https://doi.org/10.1016/j.rser.2021.111164.

[8] Akshayveer, A. Kumar, A.P. Singh, O.P. Singh, Effect of novel PCM encapsulation designs on electrical and thermal performance of a hybrid photovoltaic solar panel, Sol. Energy 205 (2020) 320–333. https://doi.org/10.1016/j.solener.2020.05.062.

[9] T. Klemm, A. Hassabou, A. Abdallah, O. Andersen, Thermal energy storage with phase change materials to increase the efficiency of solar photovoltaic modules, Energy Procedia 135 (2017) 193–202. https://doi.org/10.1016/j.egypro.2017.09.502.

[10] P. Michael Joseph Stalin, K.S. Prasad, K.P. Kumar, G. Hemadri, M. Rajesh, K.P. Kumar, Performance improvement of solar PV through the thermal management using a nano-PCM, Mater. Today Proc. 50 (2022) 1553–1558. https://doi.org/10.1016/j.matpr.2021.09.111.

[11] Y. Bannour, Y. El Alami, R. Nasrin, N.E. Moussaoui, B. Elhadi, A. Faiz, Numerical Optimization of Fin Configurations in Phase Change Material Systems for Improving Solar Panel Cooling and Electrical Efficiency, Energy Storage 7 (2025) e70241. https://doi.org/10.1002/est2.70241.

[12] M. Abd El-Hamid, G. Wei, L. Cui, C. Xu, X. Du, Three-dimensional heat transfer studies of glazed and unglazed Photovoltaic/Thermal systems embedded with phase change materials, Appl. Therm. Eng. 208 (2022) 118222. https://doi.org/10.1016/j.applthermaleng.2022.118222.

[13] A. Kazemian, A. Salari, A. Hakkaki-Fard, T. Ma, Numerical investigation and parametric analysis of a photovoltaic thermal system integrated with phase change material, Appl. Energy 238 (2019) 734–746. https://doi.org/10.1016/j.apenergy.2019.01.103.

[14] M.A. Alnakeeb, M. Shatarah, M.K. Hamza, M.A.A. Salam, H.M. Teamah, The effect of fin geometry on the thermal performance of a conical shell double tube latent storage unit, J. Energy Storage 94 (2024) 112471. https://doi.org/10.1016/j.est.2024.112471.

[15] M.A. Alnakeeb, M.A. Abdel Salam, M.A. Hassab, W.M. El-Maghlany, Influence of trapezoidal tube parameters on electrical and thermal performance of hybrid photovoltaic solar panels integrated with phase change materials, Case Stud. Therm. Eng. 65 (2025) 105641. https://doi.org/10.1016/j.csite.2024.105641.

[16] M. Hosseinzadeh, A. Salari, M. Sardarabadi, M. Passandideh-Fard, Optimization and parametric analysis of a nanofluid based photovoltaic thermal system: 3D numerical model with experimental validation, Energy Convers. Manag. 160 (2018) 93–108. https://doi.org/10.1016/j.enconman.2018.01.006.

[17] N. Narjabadifam, S. Salemi, M. Adib, S. Bozorgmehri, Techno-economic assessment of a photovoltaic module integrated with a two-layer phase change material unit, J. Energy Storage 51 (2022) 104243. https://doi.org/10.1016/j.est.2022.104243.

[18] A.S. Joshi, A. Tiwari, Energy and exergy efficiencies of a hybrid photovoltaic–thermal (PV/T) air collector, Renew. Energy 32 (2007) 2223–2241. https://doi.org/10.1016/j.renene.2006.11.013.

[19] S. Khanna, K.S. Reddy, T.K. Mallick, Performance analysis of tilted photovoltaic system integrated with phase change material under varying operating conditions, Energy 133 (2017) 887–899. https://doi.org/10.1016/j.energy.2017.05.150.

[20] A.D. Brent, V.R. Voller, K.J. Reid, ENTHALPY-POROSITY TECHNIQUE FOR MODELING CONVECTION-DIFFUSION PHASE CHANGE: APPLICATION TO THE MELTING OF A PURE METAL, Numer. Heat Transf. 13 (1988) 297–318. https://doi.org/10.1080/10407788808913615.

[21] J. Pu, J. Du, B. Zhang, F. Rong, F. Jiao, Y. Hong, Thermal management enhancement of photovoltaic panels using phase change material heat sinks with various T-shaped fins, Case Stud. Therm. Eng. 61 (2024) 104991. https://doi.org/10.1016/j.csite.2024.104991.

[22] M. Sardarabadi, M. Passandideh-Fard, Experimental and numerical study of metal-oxides/water nanofluids as coolant in photovoltaic thermal systems (PVT), Sol. Energy Mater. Sol. Cells 157 (2016) 533–542. https://doi.org/10.1016/j.solmat.2016.07.008.

[23] Y.E. Alami, H. Dahmani, F. Ouerradi, B. Zohal, R. Bendaoud, E. Baghaz, Impact of Heat Exchanger Materials on the Performance of Solar Hybrid Photovoltaic Thermal (PVT) Systems: 3D Analysis, in: B. Hajji, A. Gagliano, A. Mellit, A. Rabhi, M. Calì (Eds.), Proc. 4th Int. Conf. Electron. Eng. Renew. Energy Syst. - Vol. 2, Springer Nature, Singapore, 2025: pp. 609–619. https://doi.org/10.1007/978-981-97-9975-6_58.